Journal of Crystal Growth 498 (2018) 315–327

Contents lists available at ScienceDirect

Journal of Crystal Growth

journal homepage: www.elsevier.com/locate/crys

Identification of higher order silanes during monosilane pyrolysis using gas chromatography-mass spectrometry

Guro Marie Wyller *, Thomas J. Preston, Hallgeir Klette, Trygve Mongstad, Erik Stensrud Marstein

IFE (Institute for Energy Technology), Pb. 40, 2027 Kjeller, Norway

ARTICLE INFO

Article history:
Received 5 February 2018
Accepted 14 March 2018
Available online 30 March 2018
Communicated by G.B. Stringfellow

Keywords:
A1. Fluid flows
A1. Growth models
A1. Nucleation
A2. Growth from vapor
A3. Chemical vapor deposition processes
A3. Polysilicon production processes

ABSTRACT

There is a deficit of ways to detect higher order silane isomers during silane pyrolysis. Thus, a novel instrument utilizing gas chromatography-mass spectrometry (GC-MS) for detection of higher order silanes has been developed. The instrument enables us to separate higher order silane species using gas chromatography before they are introduced to the mass spectrometer, thereby obtaining spectra of separate isomers, rather than overlaid spectra. In this contribution we describe the details of the GC-MS system. We compare our GC-separated mass spectra of mono-, di- and trisilane to mass spectra of these species available in the literature. Further, we present mass spectra of the tetrasilane isomers *n*-tetrasilane (*n*-Si_4H_{10}), silyltrisilane (*i*-Si_4H_{10}) and cyclotetrasilane (*cyclo*-Si_4H_8) and of the pentasilane isomers *n*-pentasilane (*n*-Si_5H_{12}), silyltetrasilane (*i*-Si_5H_{12}) disilyltrisilane (*neo*-Si_5H_{12}) and cyclopentasilane (*cyclo*-Si_5H_{10}). Six of these mass spectra are previously unpublished. Based on the fragmentation pattern in the tetra- and pentasilane mass spectra, we are able to acquire mass spectra of silanes with up to eight silicon atoms. Finally, we apply the novel detection technique to a silane pyrolysis reactor to track the outlet concentration of higher order silanes as function of reactor temperature. We believe that the detection technique that we present here may open the door for validation of monosilane pyrolysis models, and thus constitute a roadmap for future research in this field.

1. Introduction

1.1. Pyrolysis of SiH_4 in solar silicon industry

Its market share of above 90% [1] makes crystalline silicon the dominating material in the photovoltaic industry. Silicon further plays an important role in the semiconductor industry and in the battery industry because of its promising characteristics as anode material in Li-ion batteries [2]. More than 80% of the polysilicon consumed by the solar industry is produced by thermal decomposition of trichlorosilane ($SiHCl_3$) [1]. This process, normally carried out in a Siemens reactor, constitutes an expensive and energy demanding step in the production of polysilicon. A recent study [3] indicates that reducing the energy consumption for solar grade silicon production by 15–17 kWh/kg-Si gives – in a CO_2 emission perspective – the same result as a 1% increase in the baseline efficiency for mono- and multicrystalline Si PV modules. Developing procedures to produce solar cells at lower energy consumption is therefore essential for reducing their energy payback time [3]. One way of reducing the overall energy consumption during solar cell production is by replacing the Siemens process (pyrolysis of trichlorosilane) by pyrolysis of gaseous monosilane [3].

Pyrolysis of gaseous monosilane (R1) converts it to solid silicon and gaseous hydrogen through the following overall reaction:

$$SiH_4\ (g) \rightarrow 2H_2\ (g) + Si(s) \qquad (R1)$$

The reaction can be carried out, for example, in a fluidized bed reactor (FBR), as is already done on industrial scale [4], or in centrifugal chemical vapor deposition (C-CVD) reactor currently being developed for industrial scale [5]. Despite their proven capability of producing polysilicon with significantly lower energy demand than the Siemens reactor [3,6,7], these monosilane based reactor technologies encounter limitations related to dust formation during the monosilane pyrolysis process [6–8]. Dust (fines) is formed when reactant gas molecules decompose homogeneously (in the gas phase), rather than heterogeneously (on a surface) [9,10]. Fines formation constitutes a competing chemical pathway to the desired solid silicon production and therefore causes a reduced chemical yield [8,11]. Moreover, fines formation leads to challenges with reactor clogging [12] and reduced material quality [11]. Overcoming these challenges requires understanding of the chemical complexity hidden underneath the overall chemical reaction (R1).

* Corresponding author.
E-mail address: guro.marie.wyller@ife.no (G.M. Wyller).

https://doi.org/10.1016/j.jcrysgro.2018.03.024
0022-0248/

A variety of studies, experimental [see e.g. 13–20] and by modelling [see e.g. 13,16, 20–27], have been conducted to broaden the understanding of the monosilane pyrolysis. It is commonly accepted that the pyrolysis occurs through a series of chemical reactions, including Si—Si bond formation and hydrogen elimination, producing silanes with increasing number of Si atoms [13,20,22,23,28,29]. Additionally, 1,2-hydrogen shifts, ring opening and ring closing lead to interconversion between different isomers within each silane family [22,23,30,31]. Many of the kinetic models of the monosilane pyrolysis process have an impressive degree of detail, some of which include hundreds of species with up to 10 Si atoms and more than one thousand chemical reactions [16,21–23,27]. The experimental works in the field, on the other hand, have a much lower degree of detail. These works are typically limited to measurements of silanes with no more than three or four silicon atoms and have a lack of differentiation between isomers [13,14,20,32]. Some experimental works include measurements of particle properties, like size distribution [13,15,16,33] and hydrogen content [13,15]. Because of the complex nature of the monosilane pyrolysis process, it is challenging to use these measures for verification of kinetic silane pyrolysis models. There are, in other words, few available methods for validating silane pyrolysis models. Therefore, despite the numerous works treating monosilane pyrolysis, a detailed understanding of the chemical complexity behind reaction (R1) remains elusive. This lack of understanding inhibits development of new technologies required to overcome the aforementioned challenges related to dust formation during monosilane pyrolysis. We seek to overcome these challenges by connecting chemical models and measurements of monosilane transformation. The measurement technique that we present in this contribution will help close the gap between model end experiment by allowing measurements of separate higher order silane isomers in monosilane pyrolysis exhaust and thus validation of detailed models of monosilane pyrolysis.

1.2. Detection and characterization of higher order silanes

Because of the relevance of production, detection and characterization of higher order silanes to solar silicon industry and other chemical industries, many works have addressed these topics. The electron ionization (EI) mass spectra of the two lowest silanes, monosilane [34,35] and disilane [36,37] were published already before 1970. Further, a method for producing higher order silanes [38] as well as for separating them by gas chromatography (GC) [39] have been demonstrated. In 1973 Féher et al. [40] briefly described the 70 eV EI mass spectra of some higher order silane isomers from trisilane to heptasilane, pointing out loss of SiH_4 as the main fragmentation mechanism. They did, however, not publish any species- or isomer-specific information. The same year, Höfler and Jannach [41] described the mass spectrum of disilyltrisilane (*neo*-Si_5H_{12}). They reported a weak signal for the molecular ion at m/z 152 and mentioned SiH_4-loss and successive H-loss as important fragmentation mechanisms. The successive H-loss leads to weak signals at all masses in intervals ranging from fully saturated silane molecules to naked Si chains [41]. In 1975, Hengge and Bauer published the mass spectrum of cyclopentasilane (*cyclo*-Si_5H_{10}) [42], showing a much higher abundance of the molecular ion (m/z 150) than in the case of disilyltrisilane (*neo*-Si_5H_{12}). Weaker signals at m/z 151–155 were attributed to the heavier Si isotopes (^{29}Si and ^{30}Si) and to deuterium. The further fragmentation mechanisms, with successive loss of SiH_4 and H, were similar to the one already described for disilyltrisilane (*neo*-Si_5H_{12}) [41]. Four years later, the cyclohexasilane mass spectrum was published [43], with a very similar fragmentation mechanism as was described for the five-membered ring. To the best of our knowledge, mass spectra of higher order silane isomers other than those mentioned here are so far unpublished. The knowledge of mass spectra of higher order silane is, in other words, sparse, partly due to inconsistent results [36,37,44] and partly due to the limited number of studies which have been published.

Bogaert et al. [45] applied in 1986 gas chromatography (GC) for detection of silanes with up to six silicon atoms in low-pressure mono- and disilane pyrolysis reactor effluent. These authors quantified the GC elutes with a thermal conductivity detector (TCD) by assuming TCD-response factors of the silanes relative to monosilane to be identical to those of alkanes relative to methane. Similar measurement techniques were used by Slootman and Parent [14] and by Odden et al. [20] also using GC combined with a TCD for measuring concentrations of H_2, SiH_4, Si_2H_6 and Si_3H_8 during thermal pyrolysis of SiH_4 diluted in hydrogen. Further, quadrupole mass spectrometry has been applied to detect higher order silanes (with up to five silicon atoms) in the products of plasma-enhanced deposition of amorphous silicon from monosilane [46–49], in products of thermal decomposition of monosilane diluted in argon [13,32,50], and in products of pyrolysis of disilane [44]. Vacuum ultraviolet (VUV) photoionization combined with time of flight (TOF) MS have been applied for measuring gas-phase products of pyrolysis of SiH_4 and Si_2H_6 [51–54], and it has proven capable of detecting higher order silanes with up to ten silicon atoms [52,53]. Tarzcay et al. [55] applied the same technique for detecting higher order silanes during melting of low temperature (5.5–300 K) SiH_4 ices. For this application, the authors were able to detect silanes with up to 19 silicon atoms [55].

The above described applications of mass spectrometry for measuring pyrolysis products do not include separation of different silane families and isomers prior to mass spectral characterization. Consequently, the acquired mass spectral data is a superposition of the mass spectra of numerous chemical species, hindering precise identification of the species. Researches applying gas chromatography, on the other hand, were able to separate species and isomers but lacked an exact method for identification. In the present contribution we show how gas chromatography and mass spectrometry can be combined as a powerful tool to separate *and* identify higher order silanes, allowing us to show resolved mass spectra of separate silane isomers. We describe the working principle of our GC-MS setup in detail. Further, we summarize previous findings regarding boiling points of higher order silane isomers and combine this information with mass spectral measurements to establish the spectra of seven separate tetra- and pentasilane isomers. Last, we demonstrate the application of our GC-MS measurement technique for tracking concentrations of separate higher order silane isomers as a function of the conditions in a silane pyrolysis reactor.

2. Experimental setup

Our GC-MS system consists of three main parts: a gas handling and loading system, a gas chromatograph (Agilent 7890B GC) and a mass spectrometer (Agilent 5977A MSD, subtype G7038). These three parts are described in the following subsections.

2.1. Gas handling and loading system

The gas handling system, which transfers the gas samples from the reactor to the GC-MS, is designed to accomplish two main tasks. First, the chemical composition of the gas must be kept constant all the way from the reactor to the GC-MS. Heated transfer lines are required in order to prevent silanes from depositing at the inner surface of the lines, because such deposition would alter the composition of the reactor effluent. On the other hand, heating the lines too much might result in chemical reactions

taking place in the transfer line. A sampling line temperature of 60 °C is chosen as a compromise between these two conflicting criteria. Second, for repeatable measurements, the injection pressure to the GC-MS must stay constant, regardless of the reactor pressure. Constant sampling pressure is ensured by an *argon piston*, consisting of a coiled tube and four pneumatic valves, coupled in series with the GC columns [56]. The argon piston is kept at the same temperature as the sampling line. Fig. 1 explains how the argon piston is used both for drawing sample gas from the reactor (Fig. 1a) and for injecting it into the GC columns (Fig. 1b) [56].

2.2. Gas chromatographic system

The purpose of the gas chromatographic (GC) system is to separate the different chemical species in a sample before they reach the mass spectrometer or other detectors. This separation allows us to study the mass spectrum of one species at a time with little interference from other species.

Fig. 2 shows how separation of the analyte gas is achieved by an Agilent 7890B GC system, including four different GC columns. The figure is somewhat simplified. A more detailed version is given in the supplementary material [57]. The GC separation columns are contained in an oven where the temperature can be set, thereby controlling the elution times of the different species. The system includes three detectors: a thermal conductivity detector [57], TCD_{perm}, for measuring the so-called *permanent* gasses; a second thermal conductivity detector, TCD_{silane}, which we use to measure SiH_4 and Si_2H_6; and a quadrupole mass selective detector (MSD) which we use to measure Si_3H_8 and larger silanes. By changing the GC-MS measurement procedure, the allocation of gases to be detected by the various detectors can be changed as desired. Using TCDs for the detection of mono- and disilane protects the MSD from the high concentrations of these species in our experiments. The TCD is a simpler and more robust detector than the mass spectrometer and can more easily be replaced when degraded by unwanted silane depositions within the detector system itself.

The main analytes of interest measured by TCD_{perm} are H_2, N_2, and Ar. The concentration of H_2 is of interest because it is a product in the overall silicon conversion (R1). Nitrogen is used as purge gas in the GC, and measuring it gives an indication of inter-sample contamination. Argon is used in the Ar piston sampling system (see Section 2.1) and measuring Ar is therefore necessary to check for un-wanted mixing of the forcing gas with the sample.

Samples are injected into the GC from a 500 µl sampling loop (Purged High Performance Mini-Diaphragm Valve, 10 ports of 0.030″, Dursan coated, Valve V1 in Fig. 2) with He carrier gas. When leaving the sampling loop, the gas is injected into a GS-CarbonPLOT column (Porous Layer Outer Tubular column, part number 115-3113) from Agilent. After the permanent gasses elute from the CarbonPLOT column, we backflush the silanes that remain in the CarbonPLOT. The permanent gasses are further separated in a HP-Molsieve column (Agilent, part number 19095P-MS0).

The two analytes of interest measured by TCD_{silane} are SiH_4 and Si_2H_6. A second 500 µl sampling loop (Purged High Performance Mini-Diaphragm Valve, 6 ports, valve V2 in Fig. 2) injects onto a split/splitless valve (SSL). This valve further injects onto a Select Silanes column (Agilent, part number CP7435), which separates the silanes. A Deans switch (Diaphragm Valve with Outboard purge, 3 Ports) at the end of the Select Silanes column diverts SiH_4 and Si_2H_6, which elute from Select Silanes together under our normal conditions, to a HP-PLOT/Q+PT column (Agilent part number 19091P-QO4PT). After the HP-PLOT/Q+PT column, the two species are well separated and detected by TCD_{silane}. Higher order silanes are sent through a restrictor before they are detected in the MSD.

2.3. Quadrupole mass spectral detector

The mass selective detector (MSD, type Agilent 5977A, subtype G7038) is a standard quadrupole mass analyzer, with adjustable electron ionization voltage. Under normal operation it is set up for electron ionization (EI) at 70 eV ionization energy. The MSD has unit mass resolution and a maximum possible mass range extending from m/z 1.2 to m/z 700. We set the upper limit of the mass range to m/z 240 for the current work. This upper mass limit allows for detection of silanes with up to nine silicon atoms. Choosing a higher value for maximum m/z will allow for detection of even higher order silanes. However, the possibility of detecting heavier compounds will come at the cost of reduced sensitivity across the entire mass range, as the sensitivity is limited by the dwell time at each m/z.

2.4. Calibration of GC-MS signals

We use three calibration standards from Matheson with known concentrations of monosilane (SiH_4), disilane (Si_2H_6), and trisilane (Si_3H_8) (see supplementary material [57]) for calibration of these three species. Helium is used as dilution gas. Silanes with more than three silicon atoms n_{Si} do appear in our measurements of the calibration standards, but the concentrations of these species in the standards are not known. Therefore, as of now we have no direct means of quantifying the signals for species with $n_{Si} \geq 4$, since the detectors' sensitivity can differ from one species to another. Attempts to compare concentrations of various species with $n_{Si} \geq 4$ *within one measurement* by comparing signal intensity is therefore beyond the scope of the current work. However, one may compare the concentration of one species across various measurements by comparing the signal intensity for that species in the various measurements.

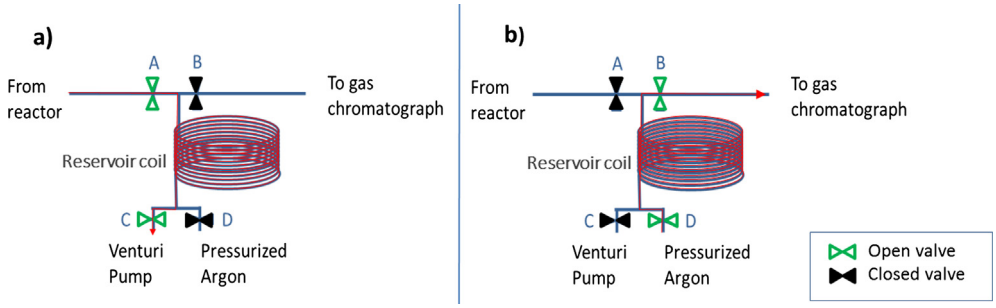

Fig. 1. Argon piston for constant sampling pressure. (a) Gas is drawn from the reactor into a reservoir coil by a Venturi pump. (b) Gas is pushed from reservoir coil to gas chromatograph by pressurized argon.

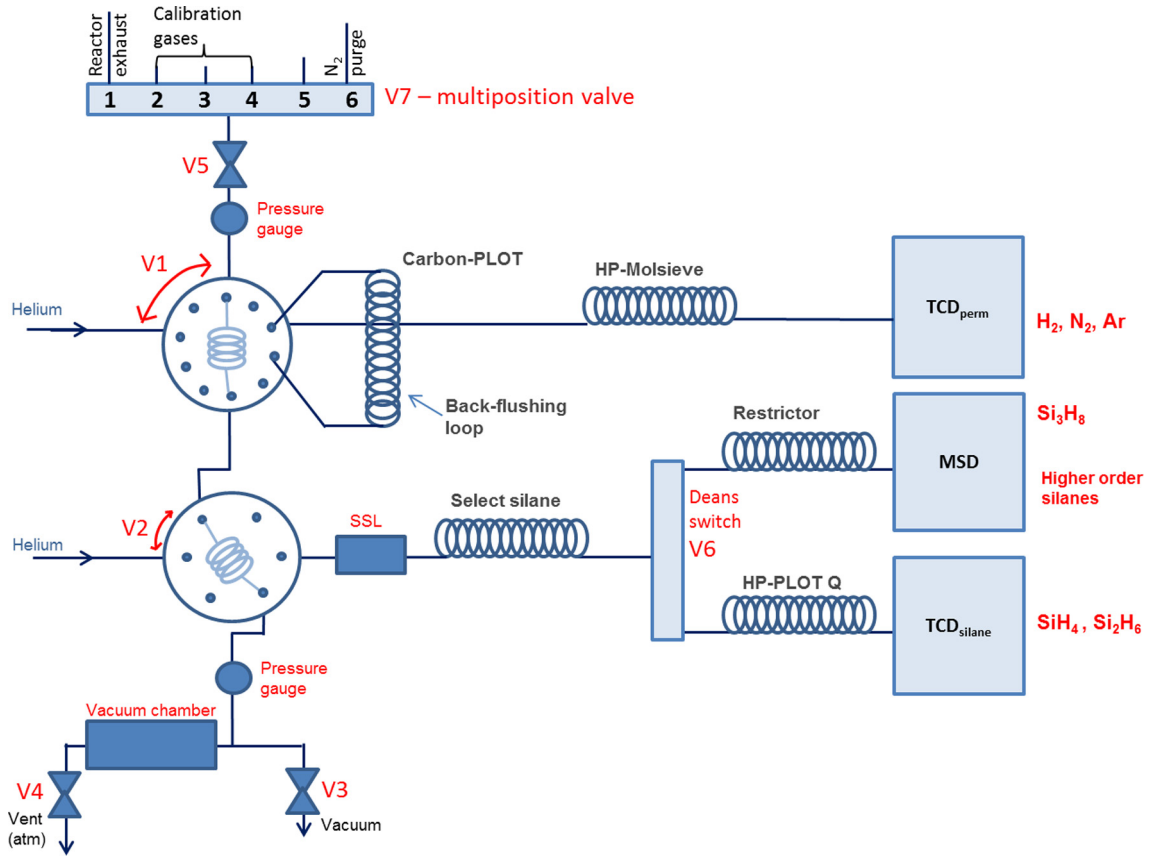

Fig. 2. Simplified drawing of the gas chromatographic system. Sample gas run through the vertical line and is injected when the two sampling loops V1 and V2 are rotated. See text for further explanation of the working principles. A more detailed figure can be found in the supplementary material [57].

2.5. Silane pyrolysis reactor

The GC-MS setup can be connected to any silane pyrolysis reactor to automatically sample the reactor exhaust. In the experiments that we describe here, a horizontal free-space reactor (FSR) with multiple heating zones was used to produce the higher silanes. Briefly stated, mixtures of H_2 and SiH_4 flow through a heated stainless steel tube with a 50 mm inner diameter in which the pyrolysis takes place. Typical total flow rates are about 4 slm (standard liter per minute), resulting in residence times about 1–5 s, depending on the number of active heating zones. Further details about the reactor can be found in our previous work [17].

3. Results & discussion

3.1. Boiling points of higher order silanes

We expect that the elution time of a silane from the GC column Select Silanes (Section 2.2) correlates with its boiling point to some degree. Among light hydrocarbon isomers with the same molecular structures as the silane isomers we are analyzing, the order of the GC retention indices [58,59], correspond very well to the boiling point order [60]. Therefore, when attempting to identify silanes based on their gas chromatographic elution times, knowledge on their boiling points is an important prerequisite. For silane isomers – as opposed to hydrocarbon isomers – boiling points have not been thoroughly addressed in the literature and are not frequently tabulated. In Fig. 3 we have collated available boiling points at 1 atm of various higher order silane isomers and plotted them as function of number of silicon atoms in the species. The numbers are also tabulated in the supplementary material [57]. We believe that this collection of data from literature is an indispensable tool for interpreting GC-MS data.

Fig. 3 includes two boiling point values for cyclopentasilane (*cyclo*-Si_5H_{10}), 173.3 °C reported by Günter [61] and 195 °C reported by Hengge and Bauer [42]. Neither of these values is frequently cited in the literature. Both boiling point values were determined with similar methods: vapor pressures at various temperatures were determined experimentally and the boiling points were determined by extrapolation of the vapor pressure curves. Günter [61] based his extrapolation on experimental values only in the range 50–83 °C and assumed the logarithm of the vapor pressure to be a linear function of 1/T in the temperature range extending up to the boiling point, about 100 °C above his experimental values. Hengge and Bauer [42], on the other hand, obtained experimental values in the range 51–157 °C. These authors report that the experimental values for the vapor pressure at high temperatures deviate slightly from a simple linear function of 1/T. Therefore, they use a more complex equation, previously applied by other authors for mono-, di and trisilane [62,63], to fit their experimental data. They report a very good agreement between the fitted equation and their experimentally obtained values [42]. Because the vapor pressures reported by Hengge and Bauer are measured far closer to the actual boiling point than those used by Günter, we assume the extrapolation by Hengge and Bauer [42] to be more trustworthy. Moreover, our observed elution time for cyclopentasilane (see Fig. 7 and Section 3.4) also supports the boiling temperature reported by Hengge and Bauer [42]. The boiling point reported by Günter [61] is therefore put in brackets in Fig. 3. Further, two slightly different values are assigned to *neo*-Si_5H_{12} in the literature [41,64]. Because there seems to be no

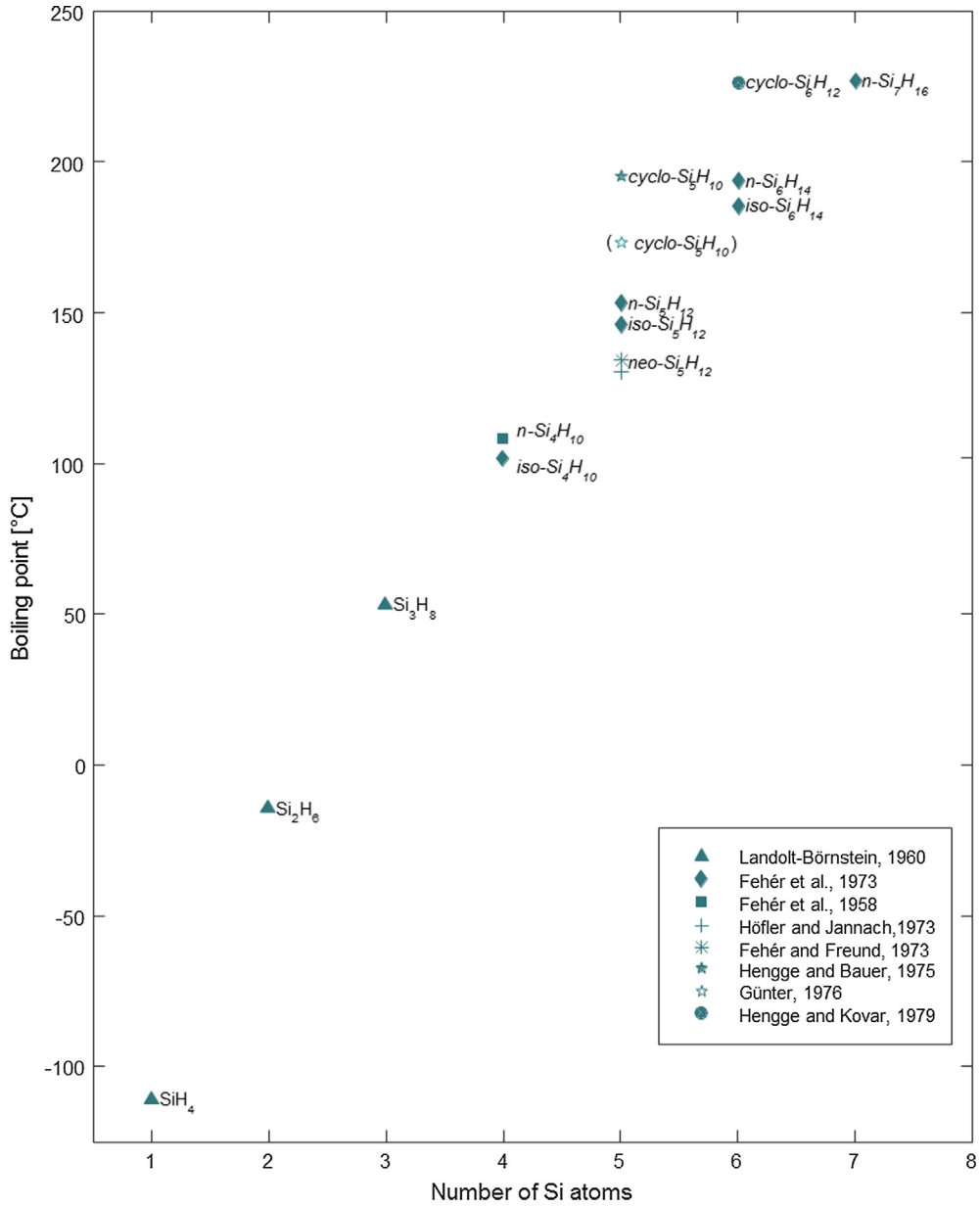

Fig. 3. Boiling points at 1 atm of various silane isomers, as found in the literature, plotted as function of numbers of Si atom n_{Si} in the species. The data is taken from Landolt-Börstein (1960) [63], Fehér et al. (1958) [65], Fehér et al. (1973) [40], Höfler and Jannach (1973) [41], Fehér and Freund (1973) [64], Hengge and Bauer (1975) [42], Günter (1976)[61] and Hengge and Kovar (1979) [43]. The boiling point of cyclopentasilane (*cyclo*-Si_5H_{10}) reported by Günter [61] is put in brackets because we find it less trustworthy than the boiling point reported by Hengge and Bauer [42] (see text).

consensus on which of the two is correct, and we find no reason to trust one more than the other: they are both included in Fig. 3.

The boiling point of cyclopentasilane, as published by Hengge and Bauer [42], is higher than the boiling points of both iso-hexasilane and n-hexasilane, meaning that we expect cyclopentasilane to elute *after* these two hexasilanes. Similarly, cyclohexasilane has a higher boiling point than n-heptasilane, meaning that we expect it to elute *after* this species. It is well known from carbon chemistry that cyclic hydrocarbons have higher boiling points [60] and higher GC retention indices [58] than non-cyclic isomers with the same number of carbon atoms.

3.2. Mass spectra of silane oligomers: Mono-, di- and trisilane

We measure only one stable isomer in each of the three lowest order silane families: mono-, di-, and trisilane. Therefore, the mass spectra corresponding to these three species are easy to identify. Fig. 4 shows the 70 eV EI mass spectra of these three species as measured by our setup as well as 70 eV EI mass spectra of the same species from the literature. For more detail on how our spectra and their uncertainties are calculated, see supplementary material [57]. The literature spectra for monosilane and trisilane are taken from the NIST WebBook [66], whereas that of disilane – which is unavailable in that database – is taken from the newest available publication including that spectrum [44].

3.2.1. Monosilane

Monosilane (Fig. 4a) has a nominal mass of 32 Da. The mass spectrum has its base peak (highest peak) at m/z 30, indicating a loss of two hydrogen atoms from the parent molecule. The peaks at m/z 28, m/z 29 and especially m/z 31 are also relatively strong, indicating that losses of four, three and one hydrogen atom(s) also

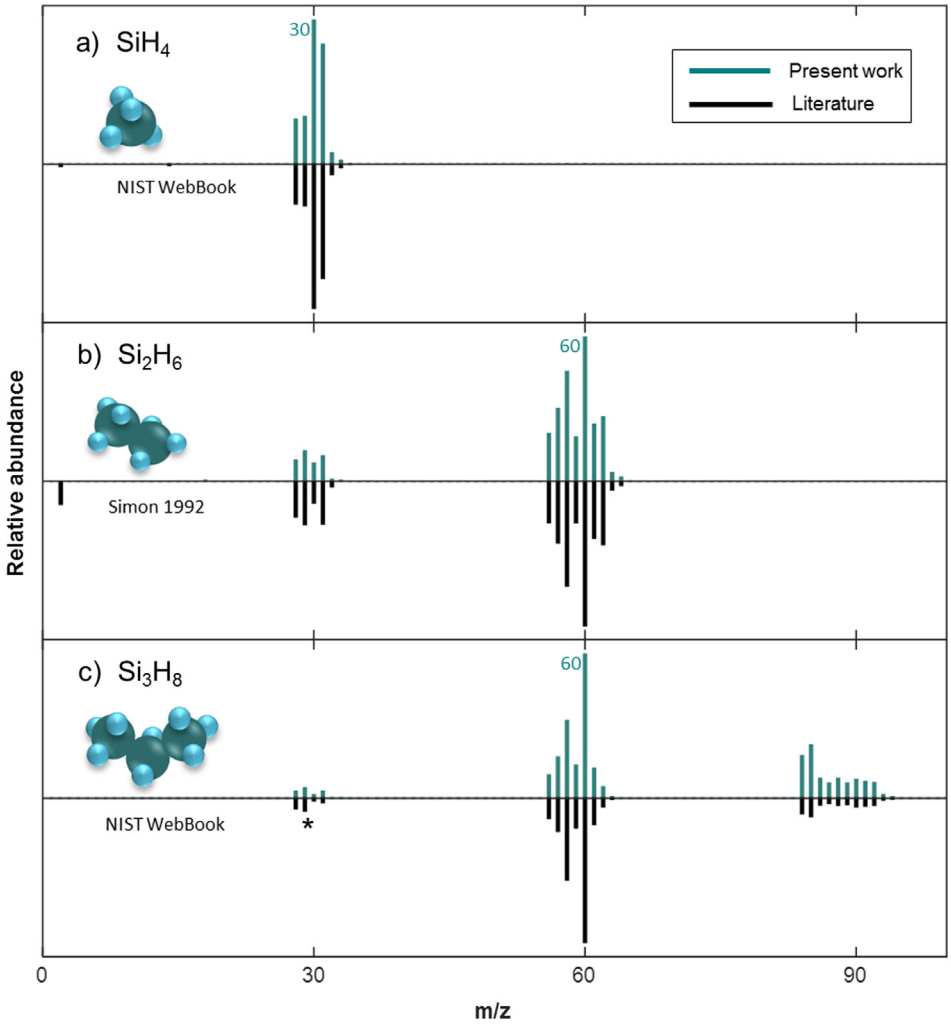

Fig. 4. 70 eV electron ionization mass spectra of the three simplest silanes: (a) monosilane (SiH_4), (b) disilane (Si_2H_6) and (c) trisilane (Si_3H_8) as measured by our setup (The data in Fig. 4 is acquired with a slightly changed version of the GC-MS shown in Fig. 2. All detectors and GC columns are the same, only the configuration of the sampling loops, the multiposition valve and the vacuum pump is changed.) (green) and as found in the literature[44,66] (black). The masses of the most abundant peaks are indicated. The asterisk near the mass spectrum of trisilane from NIST WebBook [66], shows where we have shifted the signals at *m*/*z* 28–31 (originally *m*/*z* 27–30) one mass unit upwards (see text). (For interpretation of the references to colour in this figure legend, the reader is referred to the web version of this article.)

occur. The signal corresponding to the molecular ion (*m*/*z* 32) is rather weak. The even weaker signal at *m*/*z* 33 and *m*/*z* 34 (not visible) are isotope peaks caused by the natural abundances of ^{29}Si, ^{30}Si and ^{2}H. There is good agreement between our measured mass spectrum and the mass spectrum from the literature [66] (Fig. 4a, lower pane). For our measured mass spectrum, the standard deviation for each *m*/*z* signal is within 4% of the signal strength for that *m*/*z* value. The highest uncertainties are at *m*/*z* 28 and 29, where molecular nitrogen interferes (via ^{14}N and ^{15}N). The other *m*/*z* values have standard deviations that are less than 1.3% of the signal strength. Comparing the mass spectra of monosilane and methane (CH_4) [66], which is the analog of monosilane in carbon chemistry, one notices that the methane has a much stronger molecular ion signal, indicating less extensive fragmentation. This strong tendency to fragment is a common feature for all the silanes, and has previously been pointed out by several authors [see eg. 42,51,53,55].

3.2.2. Disilane

Disilane (Fig. 4b), with a nominal mass of 62 Da, has its mass spectral base peak at *m*/*z* 60, indicating loss of two hydrogen atoms from the parent molecule. Further, there are relatively strong signals at all masses from *m*/*z* 56 to *m*/*z* 61 indicating loss of 1–6 hydrogen atoms from the parent molecule. As in monosilane, there are also isotope peaks at *m*/*z* higher than the nominal mass caused by naturally abundant silicon isotopes. Additionally, there is a group of peaks at *m*/*z* 28–32, corresponding to loss of one silicon atom and several hydrogen atoms. The loss of hydrogen atoms leads to signals ranging from the *m*/*z* value corresponding to Si_n (a naked silicon atom or chain of silicon atoms) to the *m*/*z* value corresponding to $Si_nH_{(2n+2)}$ (a fully saturated silane).

In the mass range corresponding to two silicon atoms (*m*/*z* 56–62) our standard deviation for each *m*/*z* is below 2.5% of the signal strength for that *m*/*z*. In the mass range corresponding to one silicon atom (*m*/*z* 28–32), the standard deviations are somewhat higher, with a maximum of 10% of the signal strength. The increased relative uncertainties are due to the low signal strength in this mass range. Comparing our spectrum to the spectrum by Simon et al. [44], which is the most recently published disilane spectrum available in the literature (Fig. 4b, lower pane), we find good agreement in the relative signal strength of masses corresponding to one specific number of silicon atoms. When it comes to the ratio between the group of signals corresponding to n = 1 (*m*/*z* 28–32) and the group corresponding to n = 2 (*m*/*z* 56–62),

however, there is a relatively large discrepancy between our spectrum and the spectrum by Simon et al. [44]. This discrepancy suggests a variation in the detector sensitivity as function of m/z. Other EI mass spectra of disilane obtained at 67.5 eV [36] and 70 eV [37,44] available in the literature also show large discrepancies among each other when it comes to the ratio of the signals at n = 1 and n = 2.

The mass spectrum of disilane has similarities to that of ethane [66], the analog of disilane in carbon chemistry. Both in disilane and in ethane the signals appear in groups corresponding to values from C_n to $C_nH_{(2n+n)}$. In ethane, however, there are fewer intense m/z peaks, indicating less extensive fragmentation than in disilane.

3.2.3. Trisilane

The mass spectrum of trisilane (Fig. 4c) follows a similar pattern to that of the two lower silanes: there are groups of signals at all m/z values from Si_n to $Si_nH_{(2n+2)}$ for n = [1,2,3], i.e. in the mass ranges m/z 28–32, m/z 56–62 and m/z 84–92 (and at somewhat higher masses due to the isotope peaks). Interestingly, the base peak remains at m/z 60, indicating that loss of SiH_4 (32 mass units) from the parent molecule is an important loss mechanism. This loss mechanism constitutes a difference to the carbon chemistry. In the mass spectrum of propane [66], the carbon analog to trisilane, the C_2H_5 signal is the most intense, indicating that loss of CH_3 happens frequently.

In the mass range corresponding to three silicon atoms (m/z 84–92), our standard deviation for each m/z signal is within 3% of the signal strength for that m/z value. In the mass range corresponding to two silicon atoms (m/z 56–62) our standard deviation for each m/z signal is within 5% of the signal strength for that m/z value. In the mass range corresponding to one silicon atom (m/z 28–32) our standard deviation for each m/z signal is within 14% of the signal strength for that m/z value. As in disilane, the increased relative uncertainties are due to the low signal strength in this lowest mass range. There is generally good agreement between our measured spectrum and the spectra available in literature [66] within each mass segment and poorer agreement when it comes to the ratio between segments corresponding to different number of silicon atoms. As in the case of disilane the poor agreement regarding the ratio between signal strength in segments corresponding to different number of silicon atoms suggests a possible variation in detector sensitivity as function of m/z.

In the mass segment corresponding to one silicon atom, there is a difference between the data from NIST WebBook [66] and our data. In the spectrum from the Standard Reference Database of NIST WebBook, there is a signal at m/z 27, whereas in our spectrum there is no signal below m/z 28. Considering that the lightest stable silicon isotope (^{28}Si) has an isotopic mass of 27.9769 Da, the signal at m/z 27 in the NIST WebBook spectrum must be related to some artefact. Comparison of our spectrum with the spectrum from NISTWebBook suggests that all the signals in the mass segment

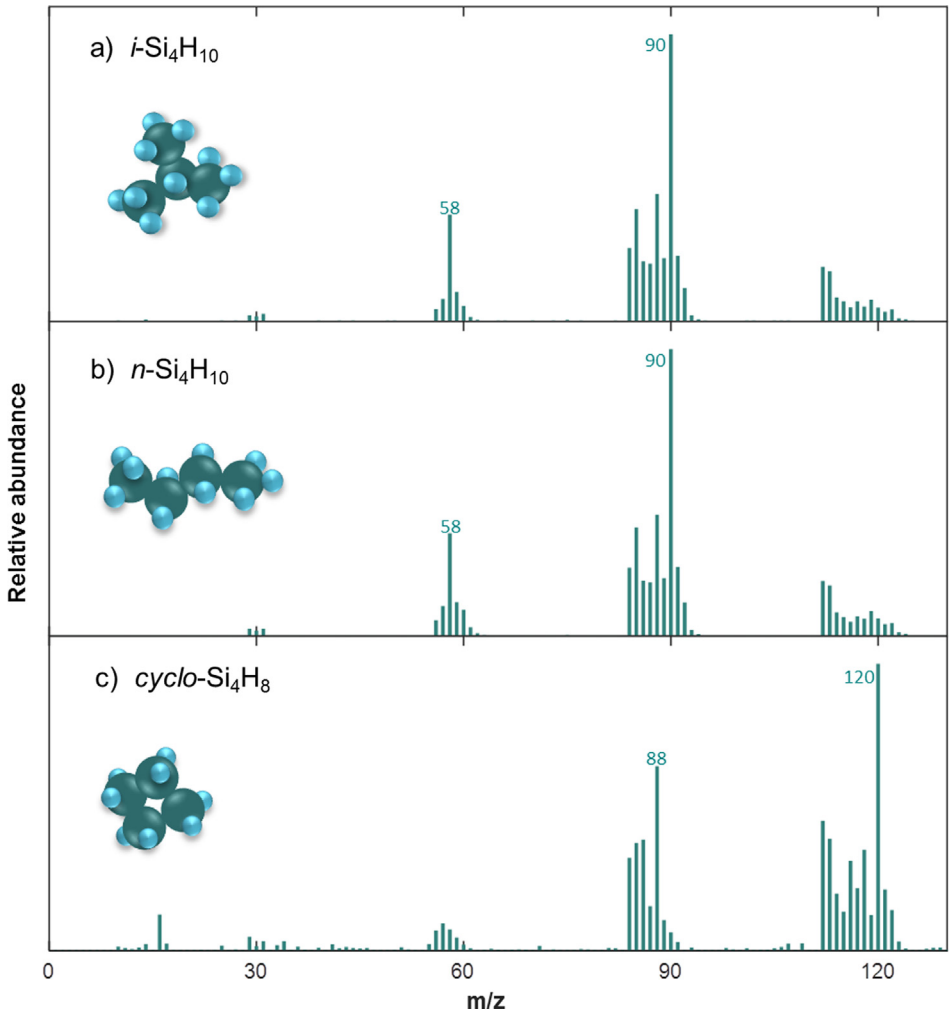

Fig. 5. 70 eV electron ionization mass spectra of three tetrasilane isomers. The masses of the most abundant peaks are indicated. We assume these species to be (a) silyltrisilane (i–Si_4H_{10}), (b) n-tetrasilane (n-Si_4H_{10}) and (c) cyclotetrasilane ($cyclo$-Si_4H_8). These molecules are indicated by the drawings.

corresponding to one silicon atom (m/z 27–30) in the spectrum in NIST WebBook may have been un-deliberately shifted one m/z unit downwards. Therefore, we have shifted those signals one mass unit upwards to m/z 28–31 in Fig. 4c (lower pane).

3.3. Mass spectra of tetrasilanes

The two most abundant tetrasilane isomers are *n*-tetrasilane (*n*-Si_4H_{10}) and silyltrisilane (*i*-Si_4H_{10}). Additionally, we expect cyclotetrasilane (Si_4H_8), which is less strained and therefore more stable than its carbon counterpart cyclobutane (C_4H_8) [67,68], to be detectable in our mixed silane samples. As indicated in Fig. 3, iso-tetrasilane has a slightly lower boiling point than n-tetrasilane [40,65], indicating that iso-tetrasilane will elute off the GC column before n-tetrasilane. The boiling point of cyclotetrasilane is not available in the literature. Based on the internal relation between the boiling points of pentasilane isomers, hexasilane isomers and isomers of the corresponding hydrocarbons (see supplementary material [57]), we have reason to assume that the boiling point of cyclotetrasilane is higher than those of the non-cyclic tetrasilanes. With this assumption (and based on the elution order which we present in Fig. 7 and discuss throughout Section 3) we tentatively assign the 70 eV EI mass spectra of the three tetrasilane isomers as shown in Fig. 5. To the best of our knowledge, these are the first published isomer-resolved EI mass spectra of the tetrasilanes.

The mass spectra of the tetrasilanes in Fig. 5 show a similar pattern as the spectra for mono-, di- and trisilane. Signals appear for m/z values in intervals ranging from Si_n to $Si_nH_{(2n+2)}$ for n = [1,2,3,4], i.e. in the mass ranges m/z 28–32, m/z 56–62, m/z 84–92 and m/z 112–122. Additionally, there are isotope peaks with m/z values up to three mass units higher than $Si_nH_{(2n+2)}$. The two non-cyclic tetrasilanes (nominal mass 122 Da) have their base peak is at m/z 90, indicating a loss of SiH_4 is a frequent fragmentation mechanism. The abundant peaks at m/z 58 in both spectra, indicate that loss of *two* SiH_4 units also happens frequently. Both these spectra have only a weak signal at the mass corresponding to the molecular ion (m/z 122). The cyclic tetrasilane (nominal mass

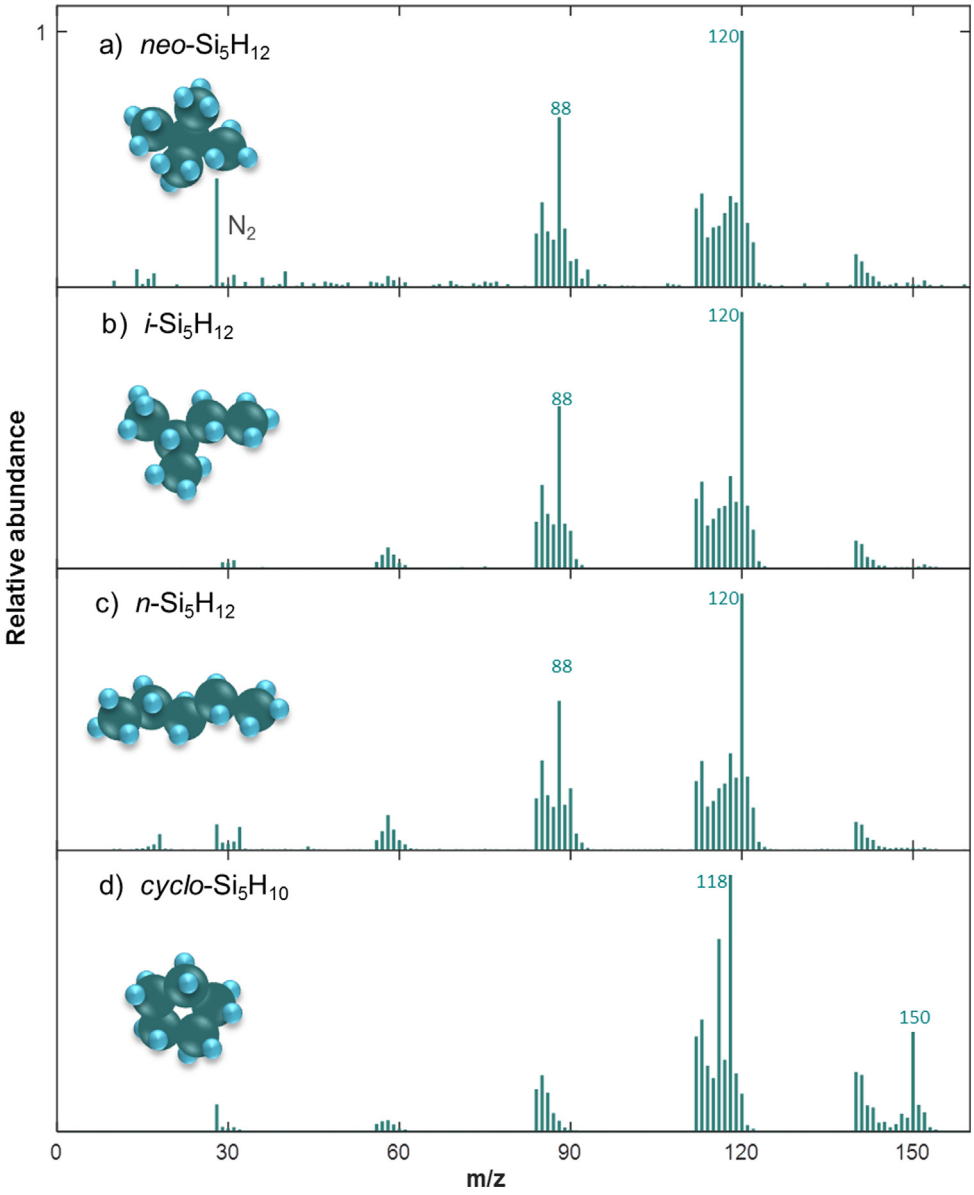

Fig. 6. 70 eV electron ionization mass spectra of four different pentasilane isomers. The masses of the most abundant peaks are indicated. The isomer from which we assume each spectra to originate are (a) disilyltrisilane (*neo*-Si_5H_{12}), (b) silyltetrasilane (*i*-Si_5H_{12}), (c) *n*-pentasilane (*n*-Si_5H_{12}) and d) cyclopentasilane (*cyclo*-Si_5H_{12}). These molecules are indicated by the drawings.

120 Da), on the other hand, has a stronger molecular ion signal (m/z 120) than its two non-cyclic counterparts. There is also a strong peak at m/z 88, pointing at loss of a SiH_4-unit as an important fragmentation mechanism also in the cyclic species. Upon comparison with the mass spectra of cyclic and non-cyclic butane [66], the carbon analogs to cyclic and non-cyclic tetrasilane, one finds a much higher abundance of the molecular ion in the mass spectrum of cyclobutane than in the mass spectra of the non-cyclic butane isomers [66]. Recognizing the same features in the mass spectra of cyclic hydrocarbons and in one of the cyclic silanes, as we do here for cyclotetrasilane (Si_4H_8), gives us guidelines for what to expect regarding the mass spectra of the larger cyclic silanes.

3.4. Mass spectra of pentasilanes

We are able to detect four pentasilane isomers in our samples. These are *n*–pentasilane (*n*-Si_5H_{12}), silyltetrasilane (*i*-Si_5H_{12}), disilyltrisilane (*neo*-Si_5H_{12}) and cyclopentasilane (*cyclo*-Si_5H_{10}) (see Fig. 6 for mass spectra and Fig. 7 for gas chromatogram). Because we identify cyclotetrasilane (*cyclo-Si_4H_8*, Fig. 5c) among the tetrasilanes, we might expect to see silylcyclotetrasilane among the pentasilanes. In the present experiments, however, the concentration of this isomer is insufficient for us to identify its mass spectrum. Silylcyclotetrasilane is therefore not included in our further analyses in this contribution. Assuming that the four detected isomers elute from the GC column in an order corresponding to their boiling points (see Fig. 3 for boiling points and Fig. 7 for gas chromatogram), we can assign their mass spectra as shown in Fig. 6.

Also in the case of pentasilanes, we recognize the same fragmentation mechanisms as for the lower order silanes: loss of SiH_4-unit(s) leads to strong peaks at m/z 120 and m/z 88 for the non-cyclic isomers. Moreover, loss of multiple hydrogen atoms gives signals at all m/z values in intervals ranging from Si_n to $Si_nH_{(2n+2)}$ for n = [1–5]. As in the case of tetrasilanes, the spectra of the cyclic species differ from the non-cyclic isomers by a more prominent peak corresponding to the molecular ion (m/z 150), and by a shift of two mass units for the other prominent peaks. For the non-cyclic isomer, the molecular ion (m/z 152) signal is small. Our mass spectrum of cyclopentasilane corresponds well to that published by Hengge and Bauer [42] in 1975 regarding relative signal strength within one Si_n mass segment (masses corresponding to the same number of silicon atoms). When it comes to the ratio among segments corresponding to different number of silicon atoms, the agreement is rather poor. As discussed in Section 3.2, a possible source could be variation in the respective sensitivities of the detectors as function of m/z.

Cyclopentasilane (*cyclo*-Si_5H_{10}) elutes after the other pentasilanes and several of the hexasilanes (see chromatogram in Fig. 7). The late elution of cyclopentasilane compared to other species corroborates our suggestion in Section 3.1 of 195 °C (as reported by Hengge and Bauer [42]) rather than 173.3 °C (as reported by Günter [61]) being a trustworthy value for the boiling point of cyclopentasilane (see Fig. 3).

3.5. Considerations on fragmentation mechanisms

The mass spectra of the three non-cyclic pentasilane isomers shown in Fig. 6 have very similar features, indicating that these species have very similar ways of fragmenting. The same holds true for the two non-cyclic tetrasilane isomers shown in Fig. 5. The similarity of the mass spectra of separate isomers marks a difference to hydrocarbons, whose various isomers have larger differences between their mass spectral patterns [66]. Despite both Si and C being group IV elements, the two elements carry several differences that can cause variations in the fragmentation behavior of hydrocarbons and silanes. First, both Si—Si bonds and H—Si bonds are significantly weaker than C—C and C—H bonds, which can lead to more extensive fragmentation in silanes than in hydrocarbons. Second, Si is more electropositive than H, whereas C is more

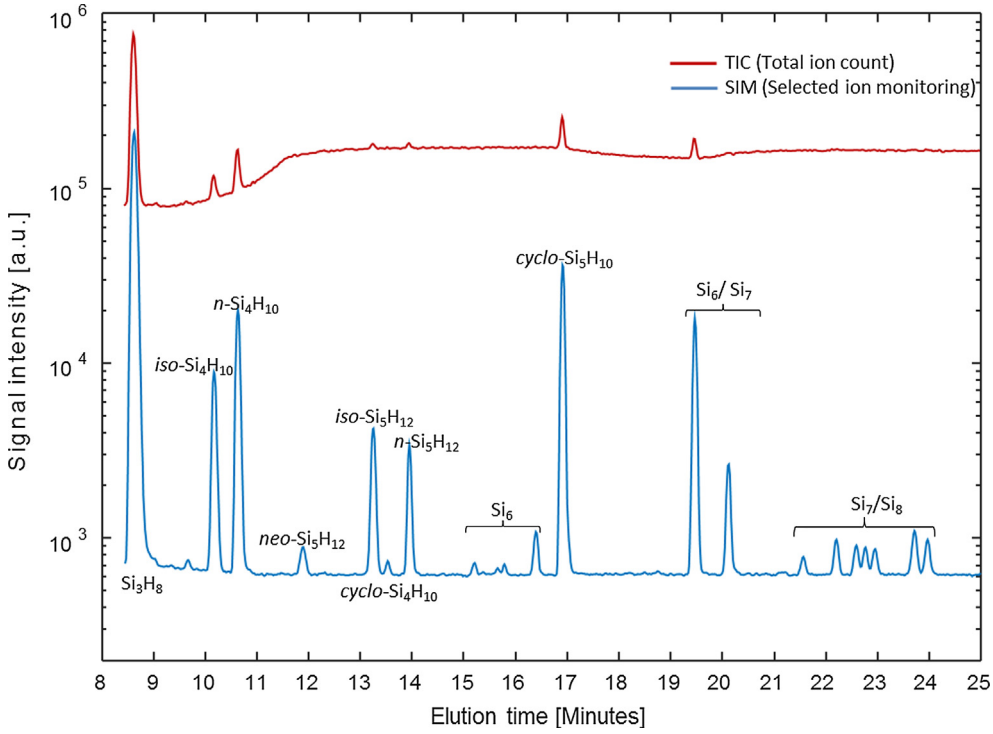

Fig. 7. Chromatograms showing the sum of the monitored ions as function of elution time for the same silane gas sample measured with TIC (total ion count) and SIM (selected ion monitoring). Note the large difference in sensitivity. The labels show the species to which the chromatographic peaks are assigned (see text).

electronegative than H. Therefore, Si_xH_y has a stronger tendency to form Si—H—Si bridges than C_xH_y has to form C—H—C bridges. George et al. [69] identified a hydrogen bridged trisilane cation structure $H_3Si—H—SiH_2—SiH_3^+$ whose energy is only a few kJ/mol higher than the classical trisilane cation $SiH_3—SiH_2—SiH_3^+$. The barrier between the two isomers is only 0.8 eV [69]. Tarczay and co-authors [55] have therefore recently suggested that the fragmentation of silanes during vacuum ultra-violet (VUV) photoionization goes via the hydrogen bridged structure. The amount of energy supplied by an incoming photon during VUV photoionization in their experiments (10.49 eV) is more than 1 eV higher than typical ionization energies for higher silanes (8.8–9.2 eV)[70]. It is therefore very likely that the classical trisilane ion can isomerize into the hydrogen bridged structure, and similarly that any higher order silane Si_nH_{2n+2} can also isomerize into the corresponding hydrogen bridged structure, which subsequently fragments through elimination of SiH_4 [55]. During electron ionization (EI), the amount of energy supplied by each electron (70 eV) is much higher than the typical photon energy used in VUV photoionization. It is therefore possible that ions also in the case of EI isomerize into the hydrogen bridged structure before they fragment further by elimination of SiH_4. The assumption that the fragmentation mechanism of all noncyclic isomers within one silane family includes the same hydrogen bridged intermediate structure can explain the similarity of the mass spectra of these isomers.

3.6. Detection of silanes with number of silicon atoms n_{Si} >5

Silanes with number of silicon atoms $n_{Si} > 5$ are mostly present at very low concentrations in our samples. In a full ion scan (TIC, total ion count) measurement in the MSD, the low signal to noise ratio causes difficulties in detecting silanes at these low concentrations. Detecting only a small selection of ions enhances the signal to noise ratio by increasing the collection time for each ion, thereby allowing for enhanced sensitivity to species at low concentration. In order to develop a selected ion monitoring (SIM) measurement, a priori knowledge of the mass spectral features of the silanes is necessary. Resolved EI mass spectra of silanes with number of silicon atoms $n_{Si} > 5$ are mostly absent in the literature (with cyclohexasilane [43], as far as we know, being the only exception), so this knowledge is not readily available.

Assuming that the fragmentation pattern that we present above for tri-, tetra- and pentasilanes holds true also for the silanes with $n_{Si} > 5$, we can deduce which masses will be abundant for the higher silanes. Implementing these masses in a SIM measurement method drastically increases the signal to noise ratio and thus the sensitivity of our measurement. Fig. 7 illustrates the increase in sensitivity by comparing the chromatogram of a standard TIC measurement to that of a SIM measurement. The ions selected for the SIM measurement are listed in the supplementary material [57].

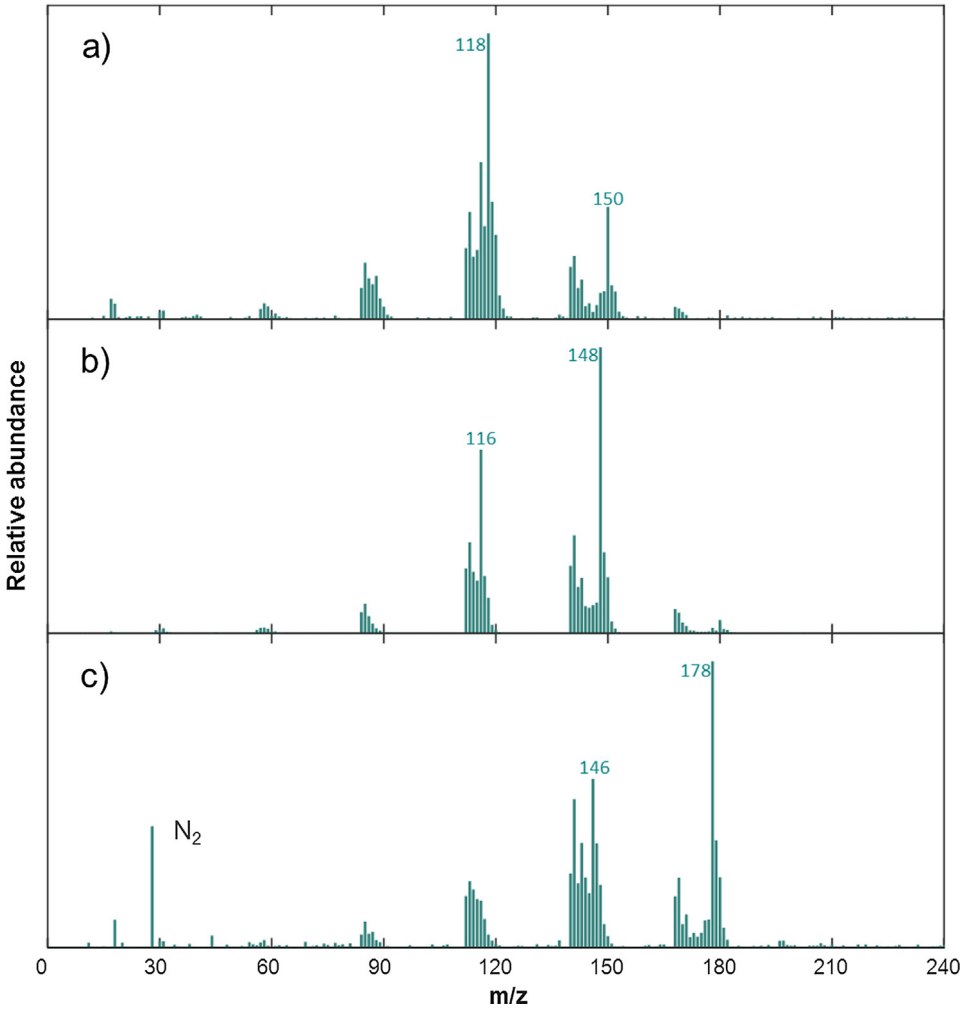

Fig. 8. 70 eV electron ionization mass spectra of three silanes, which we suggest are (a) a hexasilane (b) a heptasilane and (c) an octasilane. The masses of the most abundant peaks are indicated.

As seen by Fig. 7, several peaks appear after application of our SIM measurement. By examining full ion scans at the retention times corresponding to these peaks, they can be assigned to a silane family. Fig. 8 shows three of these spectra, which we assume to correspond to a hexasilane (182 Da), a heptasilane (212 Da) and an octasilane (242 Da). We assign each mass spectrum to a silane family primarily based on assuming loss of multiple SiH_4-units (m/z 32) from the parent molecule.

Our capability to assign with certainty isomers with $n_{Si} \geq 6$ to GC peaks is, however, limited by the way cyclic and non-cyclic species fragment and by instrument sensitivity. As we observe for cyclotetrasilane and cyclopentasilane, cyclic species have a weaker tendency to fragment and therefore have stronger signals corresponding to their parent molecular mass than the non-cyclic isomers have. Thus, we assume a *cyclic* silane Si_nH_{2n} to have a strong signal at the m/z value corresponding to its parent mass Si_nH_{2n}. When a *non-cyclic* silane $Si_{(n+1)}H_{2(n+1)+2}$, originally containing one Si atom more than the cyclic silane Si_nH_{2n}, undergoes loss of SiH_4, it is left with Si_nH_{2n}. Consequently, we expect a strong signal at the m/z value corresponding to Si_nH_{2n} also in this case. In the non-cyclic silane we expect the signals in the mass range corresponding to the full number of Si atoms ($Si_{(n+1)}$) to be rather weak. In many cases these signals are so weak that they are below or barely above the detection limit in our MSD (see e.g. Fig. 8c).

For the reasons explained above, despite the difference in total mass between the parent molecules Si_nH_{2n} and $Si_{(n+1)}H_{2(n+1)+2}$, the mass spectra of these two compounds will be rather similar. At the present, we are therefore not capable of telling the difference between the mass spectra of, e.g., a cyclic hexasilane (Si_6H_{12}) and that of a non-cyclic heptasilane (Si_7H_{16}). The assignment of the peaks and mass spectra of compounds with $n_{Si} \geq 6$ in Figs. 7 and 8 are thus uncertain. Furthermore, for silanes with $n_{Si} \geq 6$, the number of isomers increases rapidly, making the assignment of chromatographic peaks to specific species challenging. A detailed description of the mass spectra of $n_{Si} \geq 6$, and assignment of spectra to specific isomers is out of scope for this work.

3.7. Application to silane reactor monitoring

We have previously shown [17] that our GC-MS technique can be used for monitoring the presence of silanes from different silane families as function of reactor conditions. With our improved understanding of the mass spectra of separate isomers, we are now able to track concentrations of separate isomers rather than whole silane families. Fig. 9 illustrates how our measurement method can be applied for measuring outlet concentrations of separate higher order silane isomers as function of reactor temperature in a silane pyrolysis reactor. The results shown are for an inlet concentration of 10% SiH_4 in H_2. At this stage, we do not have the tools for an exact calibration of the concentration data (see Section 2.4). However, based on electron capture cross sections for hydrocarbon isomers [71], we assume that species with the same number n_{Si} of silicon atoms have very similar electron capture cross sections and therefore similar MS response factors. With this assumption, Fig. 9 indicates that among the pentasilane isomers, cyclic pentasilane is produced at the highest concentration.

Our observation is in line with results by Wong et al. [27], who have modelled silicon nanoparticle formation via automated mechanism generation. At a simulated reactor temperature 750 °C and an initial concentration of 10% SiH_4 in H_2, these authors report cyclopentasilane to be the most abundant pentasilane species. Despite their and numerous other works including detailed modelling of monosilane pyrolysis, there are few available methods for testing the modelled data. The good agreement between our measurements of silane pyrolysis exhaust and previously modelled data is therefore very promising. Aided by GC-MS measurements of separate silane isomers described here, we will be able to further compare modelled and experimental data, allowing for tuning and improvements of chemical kinetics models of monosilane pyrolysis. Developing these models is again crucial for further improvements of monosilane based silicon reactor technologies.

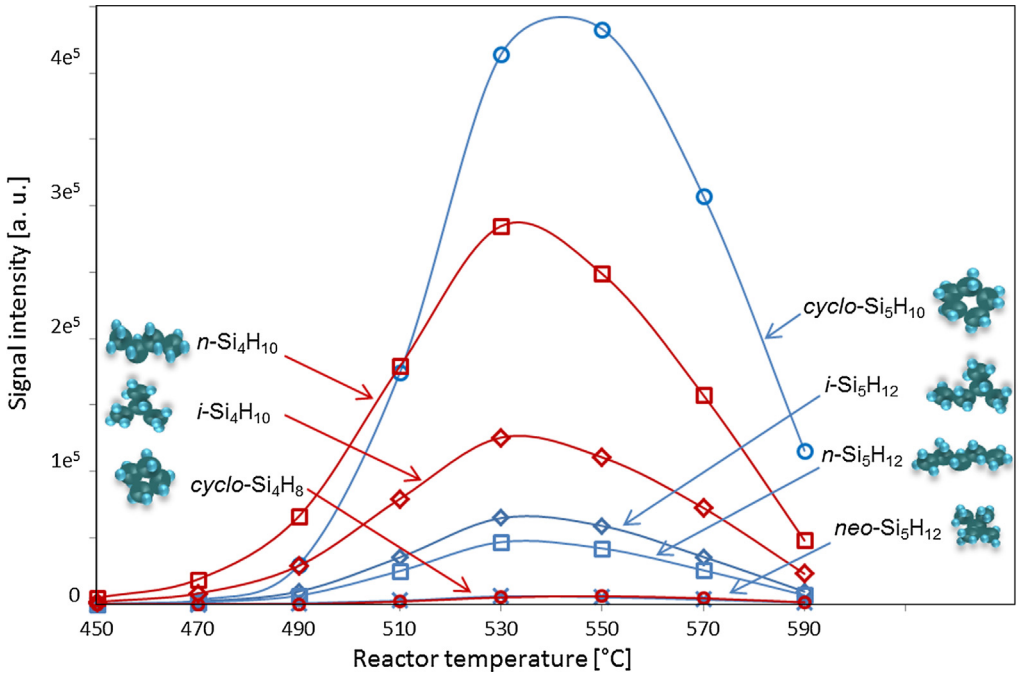

Fig. 9. Outlet concentrations (given in arbitrary units) of tetra- and pentasilane isomers as function of reactor temperature in a monosilane pyrolysis reactor. The lines are guides to the eye.

4. Conclusion

A novel instrument using gas chromatography-mass spectrometry (GC-MS) for separation and detection of higher order silanes has been demonstrated. The instrument enables us to acquire previously unpublished 70 eV EI mass spectra of separate isomers of tetra- and pentasilane. Aided by collated information on boiling points of the higher order silane species we are able to assign these spectra to specific isomers. All the silane isomers that we have studied show similar mass spectral features: for an isomer with n_{Si} silicon atoms, groups of signals appear at all m/z values in intervals ranging from Si_n to $Si_nH_{(2n+2)}$ (Si_nH_{2n} for cyclic species), i.e. from a naked chain of silicon atoms to a fully saturated silane, for $1 < n < n_{Si}$. The strongest signals in the spectra indicate loss of 32, 64 or 96 mass units from the parent mass, pointing to loss of one or more SiH_4 units (32 Da) is an important fragmentation mechanism. Mass spectra of different non-cyclic isomers with the same number n_{Si} of silicon atoms have very similar mass spectra. These mass spectra are much more similar than the mass spectra of corresponding hydrocarbon isomers with the same number n_C of carbon atoms. The similarity between the mass spectra of the silane isomers can be explained by a hydrogen-bridged state through which the fragmentation of all the isomers proceeds.

Application of our GC-MS system to track outlet concentration of higher order silane isomers in monosilane pyrolysis reactor exhaust suggests that, among the pentasilane species, cyclopentasilane is produced at the highest concentration during the pyrolysis. Our measurement and interpretation corresponds well with modelled data by Wong et al. [27]. Numerous contributions to the modelling of monosilane pyrolysis have been published. There is, however, a deficit of ways to detect higher order silane isomers during silane pyrolysis. The novel GC-MS technique we present herein opens the door for validation of monosilane pyrolysis models.

Acknowledgements

We would like to thank Marius Westgård Erichsen, Petter Lassen and Ørjan Espeseth at Matriks Kjemiske Teknologi, as well as Jesper Bennetsen for their kind cooperation and their help in the planning and construction of the GC-MS apparatus. Further, we would like to thank Werner Filtvedt at Dynatec Engineering and Stein Julsrud and Edgar Estupiñán at REC Silicon for useful discussions. We are also grateful for the funding from Norwegian Research Council through The Research Centre for Sustainable Solar Cell Technology - SUSOLTECH (NFR project no. 257639).

Appendix A. Supplementary material

Supplementary data associated with this article can be found, in the online version, at https://doi.org/10.1016/j.jcrysgro.2018.03.024.

References

[1] G. Cellere, H. Forstner, T. Falcon, M. Zwegers, J. Bernreuter, International Technology Roadmap for Photovoltaic (2016). papers2://publication/uuid/20F56C7C-3684-4039-B043-D3DE7C5293FA.
[2] M. Ashuri, Q. He, L.L. Shaw, Silicon as a potential material for Li-ion batteries: where size, geometry and structure matter, Nanoscale 8 (2016) 74–103, https://doi.org/10.1039/c5nr05116a.
[3] D. Ravikumar, B. Wender, T.P. Seager, M.P. Fraser, M. Tao, A climate rationale for research and development on photovoltaics manufacture, Appl. Energy. 189 (2017) 245–256, https://doi.org/10.1016/j.apenergy.2016.12.050.
[4] W.O. Filtvedt, T. Mongstad, A. Holt, M. Melaaen, H. Klette, Production of silicon from SiH_4 in a fluidized bed, operation and results, Int. J. Chem. React. Eng. 11 (2013) 1–12, https://doi.org/10.1515/ijcre-2012-0027.
[5] W.O. Filtvedt, H. Klette, S. Sørensen, J. Filtvedt, Low cost/high quality silicon production by centrifuge CVD reactor upscaled and hot harvest, in: EU PVSEC XXXI 2BO.1.2, Hamburg, 2015. http://doi.org/10.1007/s13398-014-0173-7.2.
[6] A. Ramos, W.O. Filtvedt, D. Lindholm, P.A. Ramachandran, A. Rodríguez, C. del Cañizo, Deposition reactors for solar grade silicon: a comparative thermal analysis of a Siemens reactor and a fluidized bed reactor, J. Cryst. Growth. 431 (2015) 1–9, https://doi.org/10.1016/j.jcrysgro.2015.08.023.
[7] W.O. Filtvedt, T. Mongstad, H. Klette, A. Holt, S. Sørensen, J. Filtvedt, Novel low cost production through centrifuge chemical vapor deposition, Silicon Chem. Sol. Ind. XII (2014).
[8] J. Li, G. Chen, P. Zhang, W. Wang, J. Duan, Technical challenges and progress in fluidized bed chemical vapor deposition of polysilicon, Chinese J. Chem. Eng. 19 (2011) 747–753, https://doi.org/10.1016/S1004-9541(11)60052-9.
[9] T. Murthy, N. Miyamoto, M. Shimbo, J. Nishizawa, Gas-phase nucleation during the thermal decomposition of silane in hydrogen, J. Cryst. Growth. 33 (1976) 1–7, https://doi.org/10.1016/0022-0248(76)90072-5.
[10] G. Hsu, R. Hogle, N. Rohatgi, A. Morrison, Fines in fluidized bed silane pyrolysis 157 (1984) 660–663.
[11] G. Bye, B. Ceccaroli, Solar grade silicon: technology status and industrial trends, Sol. Energy Mater. Sol. Cells. 130 (2014) 634–646, https://doi.org/10.1016/j.solmat.2014.06.019.
[12] W.O. Filtvedt, M. Javidi, A. Holt, M.C. Melaaen, E. Marstein, H. Tathgar, P. Ramachandran, Development of fluidized bed reactors for silicon production, Sol. Energy Mater. Sol. Cells. 94 (2010) 1980–1995, https://doi.org/10.1016/j.solmat.2010.07.027.
[13] A.A. Onischuk, A.I. Levykin, V.P. Strunin, M.A. Ushakova, R.I. Samoilova, K.K. Sabelfeld, V.N. Panfilov, Aerosol formation under heterogeneous/homogeneous thermal decomposition of silane: experiment and numerical modelling, J. Aerosol Sci. 31 (2000) 879–906, https://doi.org/10.1016/S0021-8502(99)00562-5.
[14] F. Slootman, J.-C. Parent, Homogeneous gas-phase nucleation in silane pyrolysis, J. Aerosol Sci. 25 (1994) 15–21, https://doi.org/10.1016/0021-8502(94)90178-3.
[15] J.O. Odden, P.K. Egeberg, A. Kjekshus, From monosilane to crystalline silicon, Part I: decomposition of monosilane at 690–830K and initial pressures 0.1–6.6 MPa in a free-space reactor, Sol. Energy Mater. Sol. Cells 86 (2005) 165–176, https://doi.org/10.1016/j.solmat.2004.07.002.
[16] S. Nijhawan, P.H. McMurry, M.T. Swihart, S.-M. Suh, S.L. Girshick, S.A. Campbell, J.E. Brockmann, An experimental and numerical study of particle nucleation and growth during low-pressure thermal decomposition of silane, J. Aerosol Sci. 34 (2003) 691–711, https://doi.org/10.1016/S0021-8502(03)00029-6.
[17] G.M. Wyller, T.J. Preston, T.T. Mongstad, D. Lindholm, H. Klette, Ø. Nordseth, W. O. Filtvedt, E.S. Marstein, Influence of temperature and residence time on thermal decomposition of monosilane, Energy Procedia 124 (2017) 812–822, https://doi.org/10.1016/j.egypro.2017.09.352.
[18] G.M. Wyller, T.J. Preston, H. Klette, Ø. Nordseth, T. Mongstad, W.O. Filtvedt, E.S. Marstein, Critical nucleation concentration for monosilane as function of temperature observed in a free space reactor, Energy Procedia 92 (2016) 904–912, https://doi.org/10.1016/j.egypro.2016.07.100.
[19] E.L. Petersen, M.W. Crofton, Measurements of high-temperature silane pyrolysis using SiH_4 IR emission and SiH_2 laser absorption, J. Phys. Chem. A 107 (2003) 10988–10995, https://doi.org/10.1021/jp0302663.
[20] J.O. Odden, P.K. Egeberg, A. Kjekshus, From monosilane to crystalline silicon, part II: kinetic considerations on thermal decomposition of pressurized monosilane, Int. J. Chem. Kinet. 38 (2006) 309–321, https://doi.org/10.1002/kin.20164.
[21] B.L. Slakman, H.S. Simka, H. Reddy, R.H. West, Extending reaction mechanism generator (RMG) to silicon hydride chemistry, Ind. Eng. Chem. Res. 55 (2016) 12507–12515, https://doi.org/10.1021/acs.iecr.6b02402.
[22] M.T. Swihart, S.L. Girshick, Thermochemistry and kinetics of silicon hydride cluster formation during thermal decomposition of silane, J. Phys. Chem. B 103 (1999) 64–76, https://doi.org/10.1021/jp983358e.
[23] S.L. Girshick, M.T. Swihart, M.R. Mahajan, S. Nijhawan, Numerical modeling of gas-phase nucleation and particle growth during chemical vapor deposition of silicon, J. Electrochem. Soc. 147 (2000) 2303–2311, http://jes.ecsdl.org/content/147/6/2303.
[24] H.Y. Dang, M.T. Swihart, Computational modeling of silicon nanoparticle synthesis: I. A general two-dimensional model, Aerosol Sci. Technol. 43 (2009) 250–263, https://doi.org/10.1080/02786820802598059.
[25] W.J. Menz, M. Kraft, A new model for silicon nanoparticle synthesis, Combust. Flame. 160 (2013) 947–958, https://doi.org/10.1016/j.combustflame.2013.01.014.
[26] P. Zhang, Effect of operation parameters on fines formation during thermal decomposition of silane, Sol. Energy 155 (2017) 75–81, https://doi.org/10.1016/j.solener.2017.06.019.
[27] H. Wong, X. Li, M.T. Swihart, L.J. Broadbelt, Detailed kinetic modeling of silicon nanoparticle formation chemistry via automated mechanism generation, J. Phys. Chem. A 108 (2004) 10122–10132, https://pubs.acs.org/doi/abs/10.1021/jp049591w.
[28] A.J. Adamczyk, M.-F. Reyniers, G.B. Marin, L.J. Broadbelt, Kinetic correlations for H_2 addition and elimination reaction mechanisms during silicon hydride pyrolysis, Phys. Chem. Chem. Phys. 12 (2010) 12676–12696, https://doi.org/10.1039/c0cp00666a.
[29] A.A. Onischuk, V.N. Panfilov, Mechanism of thermal decomposition of silanes, Russ. Chem. Rev. 70 (2001) 321–332, https://doi.org/10.1070/RC2001v070n04ABEH000603.
[30] A.J. Adamczyk, M.F. Reyniers, G.B. Marin, L.J. Broadbelt, Exploring 1,2-hydrogen shift in silicon nanoparticles: reaction kinetics from quantum chemical calculations and derivation of transition state group additivity

database, J. Phys. Chem. A. 113 (2009) 10933–10946, https://doi.org/10.1021/jp9062516.
[31] A.J. Adamczyk, M.F. Reyniers, G.B. Marin, L.J. Broadbelt, Hydrogenated amorphous silicon nanostructures: novel structure-reactivity relationships for cyclization and ring opening in the gas phase, Theor. Chem. Acc. 128 (2011) 91–113, https://doi.org/10.1007/s00214-010-0767-x.
[32] A.A. Onischuk, V.P. Strunin, M.A. Ushakova, V.N. Panfilov, Studying of silane thermal decomposition mechanism, Int. J. Chem. Kinet. 30 (1998) 99–110, https://onlinelibrary.wiley.com/doi/abs/10.1002/%28SICI%291097-4601%281998%2930%3A2%3C99%3A%3AAID-KIN1%3E3.0.CO%3B2-O.
[33] R. Körmer, M.P.M. Jank, H. Ryssel, H.-J. Schmid, W. Peukert, Aerosol synthesis of silicon nanoparticles with narrow size distribution—Part 1: experimental investigations, J. Aerosol Sci. 41 (2010) 998–1007, https://doi.org/10.1016/j.jaerosci.2010.05.007.
[34] H. Neuert, H. Clasen, Massenspektrometrische Untersuchung von SH_2, SeH_2, PH_3, SiH_4 und GeH_4, Zeitschrift Für Naturforsch. 7 (1951) 410–416.
[35] F.E. Saalfeld, H. Svec, The mass spectra of volatile hydrides. I. The monoelemental hydrides of the group IVB and VB elements, Inorg. Chem. 2 (1963) 46–50, https://doi.org/10.1021/ic50005a014.
[36] F.E. Saalfeld, H.J. Svec, The mass spectra of volatile hydrides. 11. Some higher hydrides of the group IVB and VB elements, Inorg. Chem. 2 (1963) 50–53, https://doi.org/10.1021/ic50005a015.
[37] P. Potzinger, F.W. Lampe, An electron impact study of ionization and dissociation of monosilane and disilane, J. Phys. Chem. 46 (1969) 3912–3917, https://doi.org/10.1021/j100845a059.
[38] F. Fehér, D. Schinkitz, J. Scaaf, Ein Verfaren zur Herstellung höherer Silane, Zeitschrift Für Anorg. Und Allg. Chemie. 383 (1971).
[39] F. Fehér, H. Strack, Die gaschromatografische Trennung von Siliciumwasserstoffen an Squalan-Kieselgur-Trennsäulen, Naturwissenschaften. 17 (1963) 570–571.
[40] F. Fehér, P. Hädicke, H. Frings, Beitrage zur Chemie des Siliciums und Germaniums XXIII(1) Physicalisch-chemische Eigenschaften der Silane von Trisilan bis Heptasilan, Inorg. Nucl. Chem. Lett. 9 (1973) 931–936.
[41] F. Höfler, R. Jannach, Zur Kenntnis des Neopentasilanes, Inorg. Nucl. Chem. Lett. 1 (1973) 723–725.
[42] V.E. Hengge, G. Bauer, A. Chemie, T. Itochschule, O. Mit, Darstellung und Eigenschaften von Cyclopentasilan, Monatshefte Für Chemie. 512 (1975) 503–512.
[43] E. Hengge, D. Kovar, Darstellung und Characterisierung von Cyclohexasilan Si_6H_{12}, Zeitschrift Für Anorg. Und Allg. Chemie. 456 (1979) 123–130.
[44] J. Simon, R. Feurer, A. Reynes, R. Morancho, Thermal dissociation of disilane: quadrupole spectrometry investigation, J. Anal. Appl. Pyrolysis 24 (1992) 51–59, https://doi.org/10.1016/0165-2370(92)80004-6.
[45] R.J. Bogaert, R.E. Rocheleau, B.N. Baron, Gas chromatographic determination of silanes, J. Chromatogr. Sci. 24 (1986) 109–112, https://doi.org/10.1093/chromsci/24.3.109.
[46] S. Vepřek, K. Schopper, O. Ambacher, W. Rieger, M.G.J. Vepřek-Heijman, Mechanism of cluster formation in a clean silane discharge, J. Electrochem. Soc. 140 (1993) 1935–1942, http://jes.ecsdl.org/content/140/7/1935.
[47] S. Vepřek, M. Heintze, The mechanism of plasma-induced deposition of amorphous silicon from silane, Plasma Chem. Plasma Process 10 (1990) 3–26, https://link.springer.com/article/10.1007/BF01460445.
[48] J.J. Wagner, S. Vepřek, Kinetic study of the heterogeneous Si/H system under low-pressure plasma conditions by means of mass spectrometry, Plasma Chem. Plasma Process. 2 (1982) 95–107, https://link.springer.com/article/10.1007/BF00566860.
[49] G. Turban, Y. Catherine, B. Grolleau, Mass spectrometry of a silane glow discharge during plasma deposition of a-Si: H films, Thin Solid Films 67 (1980) 309–320, https://doi.org/10.1016/0040-6090(80)90464-2.
[50] A.A. Onischuk, V.P. Strunin, M.A. Ushakova, V.N. Panfilov, On the pathways of aerosol formation by thermal decomposition of silane, J. Aerosol Sci. 28 (1997) 207–222, https://doi.org/10.1016/S0021-8502(96)00061-4.
[51] S.D. Chambreau, J. Zhang, VUV photoionization time-of- flight mass spectrometry of flash pyrolysis of silane and disilane, Chem. Phys. Lett. 343 (2001) 482–488, https://doi.org/10.1016/S0009-2614(01)00739-4.
[52] K. Tonokura, T. Murasaki, M. Koshi, Diagnostics of the gas-phase thermal decomposition of Si_2H_6 using vacuum ultraviolet photoionization, Chem. Phys. Lett. 319 (2000) 507–511, https://doi.org/10.1016/S0009-2614(00)00165-2.
[53] K. Tonokura, T. Murasaki, M. Koshi, Formation mechanism of hydrogenated silicon clusters during thermal decomposition of disilane, J. Phys. Chem. B 106 (2002) 555–563, https://doi.org/10.1021/jp015523n.
[54] K. Yoshida, K. Matsumoto, T. Oguchi, K. Tonokura, M. Koshi, Thermal decomposition mechanism of disilane, J. Phys. Chem. A 110 (2006) 4726–4731, https://doi.org/10.1021/jp055280p.
[55] G. Tarczay, M. Förstel, P. Maksyutenko, R.I. Kaiser, Formation of higher silanes in low-temperature silane (SiH_4) ices, Inorg. Chem. 55 (2016) 8776–8785, https://doi.org/10.1021/acs.inorgchem.6b01327.
[56] M.K. Park, H.M. Cho, J.C. Nam, J. Kim, K.R. Kim, A simple interface for a gas chromatography system for air samples in sub-ambient pressure, Bull. Korean Chem. Soc. 22 (2001) 1273–1276.
[57] Supplementary Material.
[58] J. Bermejo, M.D. Guillén, Prediction of gas chromatographic retention indices of linear, branched, and cyclic alkanes from their physicochemical properties, J. High Resolut. Chromatogr. Chromatogr. Commun. (1984) 191–195, https://onlinelibrary.wiley.com/doi/pdf/10.1002/jhrc.1240070404.
[59] M.S.D.C. NIST, S.E. Stein, Retention Indices, in: NIST Chem. WebBook, NIST Stand. Ref. Database Number 69, Eds. P.J. Linstrom W.G. Mallard, National Institute of Standards and Technology, 2018. http://doi.org/10.18434/T4D303, (retrieved February 1, 2018).
[60] R.L. Brown, S.E. Stein, Boiling Point Data, in: NIST Chem. WebBook, NIST Stand. Ref. Database Number 69, Eds. P.J. Linstrom W.G. Mallard, 2018. http://doi.org/10.18434/T4D303, (retrieved February 1, 2018).
[61] W. Günter, Beitäge zur Chemie des Cyclopentasilans, Matematisch-Naturwissenschafliches Fakultät, Universität zu Köln, 1976.
[62] E. Hengge, H. Keller-Rudek, D. Koschel, U. Krüeke, P. Merlet, Gmelin Handbook of Inorganic Chemistry - Si Supplementary volume B1, 8th ed., Springer-Verlag, Berlin-Heidelberg-Newyork, Würzburg, 1982.
[63] Zahlenwerte Landolt-Börstein, und Funktionen aus Physik Chemie Astronomie Geophysik Technik, 6, Vol. 2, Springer-Verlag, Heidelberg, 1960.
[64] F. Fehér, R. Freund, Contributions to the chemistry of silicon and germanium, xxii (i) new silanes, bromosilanes and phenylsilanes, Inorg. Nucl. Chem. Lett. 9 (1973) 937–940, https://doi.org/10.1016/0020-1650(73)80130-8.
[65] F. Fehér, H. Keller, G. Kuhlbörsch, H. Luhleich, Isomerie in der Silan-reihe, Angew. Chemie. 70 (1958) 402.
[66] M.S.D.C. NIST, S.E. Stein, Mass Spectra, in: NIST Chem. WebBook, NIST Stand. Ref. Database Number 69, Eds. P.J. Linstrom W.G. Mallard, National Institute of Standards and Technology, Gaithersburg MD, 2018. http://doi.org/10.18434/T4D303, (retrieved February 1, 2018).
[67] F. Sax, The ground-state structure of cycltotrasilane, Chem. Phys. Lett. 127 (1986) 163–168.
[68] W.W. Schoeller, T. Dabisch, Anomaly in the ring strain behaviour of cyclopropane, cyclobutane, and cyclopentane, compared with their silicon analogues; a theoretical study, J. Chem. Soc., Chem. Commun. (1985) 1706–1707, https://doi.org/10.1039/c39850001706.
[69] M.A.R. George, M. Savoca, O. Dopfer, Infrared spectrum of the $Si_3H_8^+$ cation: evidence for a bridged isomer with an asymmetric three-center two-electron Si-H-Si bond, Chem. – A European Journal 19 (2013) 15315–15328, https://doi.org/10.1002/chem.201302189.
[70] H. Bock, W. Ensslin, F. Fehér, R. Freund, Photoelectron spectra and molecular properties. LI. 1–3 ionization potentials of silanes Si, H_{2n+2}, J. Am. Chem. Soc. 98 (1976) 668–674, https://doi.org/10.1021/ja00419a006.
[71] Y.-K. Kim, K.K. Irikura, M.E. Rudd, M.A. Ali, M. Stone, Electron-Impact Cross Sections for Ionization and Excitation Database, in: P.J. Linstrom W.G. Mallard, (Eds.), NIST Chem. WebBook, NIST Stand. Ref. Database Number 69, NIST Physical Measurement Laboratory, 2018. https://www.nist.gov/pml/electron-impact-cross-sections-ionization-and-excitation-database, (retrieved February 1, 2018).